P H Y S I C A L   R E V I E W   L E T T E R S

High-Fidelity Readout of Trapped-Ion Qubits

A. H. Myerson, D. J. Szwer, S. C. Webster, D. T. C. Allcock, M. J. Curtis, G. Imreh, J. A. Sherman, D. N. Stacey,
A. M. Steane, and D. M. Lucas

Department of Physics, University of Oxford, Clarendon Laboratory, Parks Road, Oxford OX1 3PU, United Kingdom
(Received 12 February 2008; published 23 May 2008)

We demonstrate single-shot qubit readout with a fidelity sufficient for fault-tolerant quantum computation. For an optical qubit stored in $^{40}\text{Ca}^+$ we achieve 99.991(1)% average readout fidelity in 10^6 trials, using time-resolved photon counting. An adaptive measurement technique allows 99.99% fidelity to be reached in 145 μs average detection time. For $^{43}\text{Ca}^+$, we propose and implement an optical pumping scheme to transfer a long-lived hyperfine qubit to the optical qubit, capable of a theoretical fidelity of 99.95% in 10 μs. We achieve 99.87(4)% transfer fidelity and 99.77(3)% net readout fidelity.

A quantum computer (QC) requires qubits which can be prepared and measured accurately, and made to interact through high-quality quantum logic gates. Successful fault-tolerant operation requires certain minimum thresholds for the fidelity of state preparation, logic gates, and state measurement. Qubit readout is vital, not only for the final output of the QC, but for the error-correction essential for its operation. There is a trade-off between the error rate permitted and the number of extra qubits required to achieve fault-tolerant quantum error correction (QEC), but typical studies require errors to be below $\sim 10^{-3}$ for realistic implementations [1,2]. A correction network typically uses more gates than individual qubit readouts, so readout error is less critical than gate error [2]. On the other hand, precise readout can be used to compensate for gate error. It is also crucial in a measurement-based QC [3].

Trapped-ion QC approaches generally use qubits based either on a hyperfine transition within the ground atomic level [4–8], or on an optical transition between ground and metastable states [9]. State preparation is implemented by optical pumping. State measurement is achieved by repeatedly exciting a cycling transition which involves one of the qubit states but not the other, and measuring whether or not the ion fluoresces [10]. The accuracy with which the measurement can be performed depends on the rate at which fluorescence photons can be detected for the "bright" qubit state, compared with the rate at which the "dark" state gets pumped to the bright manifold (e.g., by off-resonant excitation), or vice versa. The fact that many fluorescence photons can typically be emitted by the ion before the undesired pumping process occurs allows for high-fidelity single-shot measurement even though the absolute photon collection efficiency can be poor (typically $\sim 0.1\%$). Measurement fidelities of 98%–99% have been reported [4,6,7,9]. In recent work, an optical qubit was measured indirectly by repetitive measurement on an ancilla qubit held in the same ion trap, yielding a fidelity of 99.94% in ~ 12 ms [11].

In this Letter, we report *direct* high-fidelity measurement of first an optical qubit stored in the $(4S_{1/2}, 3D_{5/2})$

levels [12] of a single $^{40}\text{Ca}^+$ ion (Fig. 1, right) and second a hyperfine qubit stored in the $S_{1/2}$ ($F = 3, F = 4$) sublevels of a $^{43}\text{Ca}^+$ ion (Fig. 3, right), where we first map the hyperfine qubit to the $^{43}\text{Ca}^+$ optical qubit. Readout is achieved by driving the ($S_{1/2} \leftrightarrow P_{1/2} \leftrightarrow D_{3/2}$) manifold and detecting the fluorescence from the $P_{1/2} \rightarrow S_{1/2}$ decay: fluorescence indicates the qubit was initially in the bright $S_{1/2}$ state, absence of fluorescence that the qubit was in the dark metastable $D_{5/2}$ state (lifetime $\tau = 1168(7)$ ms [13]). We discuss state inference by simple photon-count thresholding and by maximum likelihood methods using time-resolved detection. The latter are applicable to a wide range of physical qubits [14].

For the $^{40}\text{Ca}^+$ measurements, a single ion is held in a Paul trap [13], Doppler cooled on the $S_{1/2} \leftrightarrow P_{1/2}$ transition by a 397 nm laser and repumped on $D_{3/2} \leftrightarrow P_{1/2}$ by an 866 nm laser. A photomultiplier (PMT) detects fluorescence from the ion with a net efficiency 0.22(2)%. The ratio of ion fluorescence to background scattered laser light has a maximum value ≈ 690 at low 397 nm intensity, but optimum readout fidelity is achieved at higher intensity because the increased fluorescence can be detected more rapidly compared with τ. Mean photon-count rates for fluorescence (R_B) and background (R_D) in this experiment were $R_B = 55\,800$ s^{-1} and $R_D = 442$ s^{-1} (including the PMT dark count rate of 8.2 s^{-1} at 20 °C).

The experimental sequence consists of preparing and measuring each qubit state in turn, and comparing the measurement outcome with the known preparation. To prepare the $D_{5/2}$ "shelf" state a 393 nm beam is switched on to drive $S_{1/2} \leftrightarrow P_{3/2}$ for 1 ms; spontaneous decay populates $D_{5/2}$ (the 866 nm beam is left on to empty $D_{3/2}$). The rate of transfer to the shelf was measured to be $[12(2) \ \mu\text{s}]^{-1}$. The 393 nm beam is extinguished and, 20(2) μs later, we start to collect PMT counts. Photons are counted for a bin time of 2 ms, which is divided into 200 sub-bins of duration $t_s = 10 \ \mu$s. Two alternately gated 10 MHz counters are used, so that there is negligible (< 50 ns) dead time between sub-bins. The counts n_i from each sub-bin i are available to the control computer
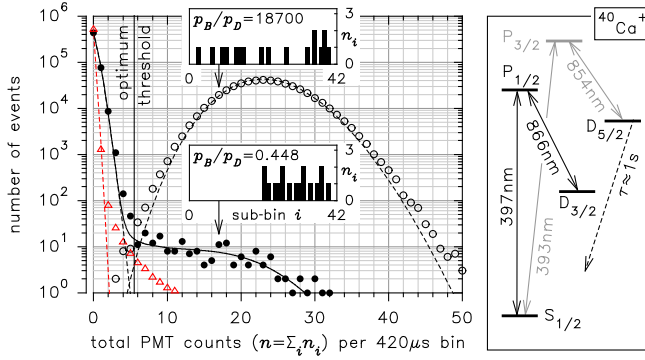
FIG. 1 (color online). $^{40}Ca^+$ photon-count histograms with $t_b = 420$ μs, for bright $S_{1/2}$ state (○) and dark $D_{5/2}$ state (●) preparations. Above-threshold events in the dark histogram give ϵ_D; below-threshold events in the bright histogram give ϵ_B. Insets show time-resolved counts for two individual 17-photon events, one from each histogram, with likelihood ratios p_B/p_D. A PMT dark count histogram is also shown (△), normalized to the same area. Dashed curves are Poisson distributions with the same means as the histograms. The solid curve is the expected $D_{5/2}$ distribution taking into account spontaneous decay.

~5 μs after the end of the sub-bin, should they be required for real-time processing, and are recorded in time order. Next, the ion is prepared in $S_{1/2}$ by driving $D_{5/2} \leftrightarrow P_{3/2}$ for ~3 ms with an 854 nm laser beam, after which fluorescence is collected for a second 2 ms bin.

This sequence was repeated to give $2^{20} \approx 10^6$ trials, in half of which the ion was prepared in the dark $D_{5/2}$ state and in half of which it was prepared in the bright $S_{1/2}$ state. We define the average readout error to be $\epsilon = \frac{1}{2}(\epsilon_B + \epsilon_D)$, where ϵ_B is the fraction of experiments in which an ion prepared in the bright state was detected to be dark, and similarly for ϵ_D. In the case of the dark state experiments, there are two small preparation errors arising from (i) the finite shelving rate of the 393 nm laser and (ii) the probability of spontaneous decay during the 20 μs delay between state preparation and the start of the detection period. These give a contribution to ϵ_D of (12 μs + 20 μs)$/\tau = 0.28(2) \times 10^{-4}$. Known state preparation errors for the bright state are negligible, so the net contribution to ϵ is $0.14(1) \times 10^{-4}$. Values of ϵ given below are after subtraction of this quantity.

Histograms of the number of photons $n = \sum_{i=1}^{N} n_i$ collected for the bright and dark state preparations are shown in Fig. 1. Here the first $N = 42$ sub-bins of the detection period were summed for a total detection time of $t_b = Nt_s = 420$ μs; this choice of t_b and a threshold at $n_c = 5\frac{1}{2}$ counts optimize the discrimination between the bright and dark histograms. The error ϵ as a function of t_b is shown in Fig. 2, for $N = 1 \ldots 100$. As t_b increases, ϵ first drops rapidly due to decreasing overlap between the two histograms, to a minimum $\epsilon = 1.8(1) \times 10^{-4}$ at $t_b = 420$ μs, then rises slowly because of the increasing probability of decay from $D_{5/2}$ during t_b.

At the optimum t_b, the majority of the error is due to the above-threshold events in the dark histogram: $\epsilon_D = 3.2(3) \times 10^{-4}$. These mostly arise due to spontaneous decay during t_b, but we also observe above-threshold events from non-Poissonian PMT dark counts. A PMT dark count distribution is also shown in Fig. 1: the highly non-Poissonian tail in the histogram probably arises as a result of cosmic rays [15]. The slow time scale of luminescence in the PMT envelope excited by the cosmic rays makes it difficult to eliminate these events entirely. We estimate that, for the threshold method, cosmic ray events account for ~20% of ϵ_D.

The threshold method does not make use of the arrival-time information of the photons. Using this information, we can hope to identify some of the events where decay from $D_{5/2}$ occurs during t_b: we may detect $>n_c$ total counts, but if these are clustered near the end of the bin this suggests a decay event rather than a bright ion (compare Fig. 1 insets). The use of time-resolved measurement in the context of qubit readout was suggested in [4] and modeled theoretically in [14,16]; we follow a similar maximum likelihood treatment to Langer [16].

We calculate the likelihood p_B that a given set of sub-bins $\{n_i\}$ could have been generated by a bright ion, and compare this with the likelihood p_D that $\{n_i\}$ arose from an ion that was dark at the start of the detection period. If $p_B > p_D$ we infer that the ion was bright and vice versa. $p_B = P(\{n_i\}|\text{bright})$ is given simply by the product of probabilities $p_B = \Pi_{i=1}^{N} B(n_i)$ where $B(n_i)$ is the probability of observing n_i counts from a bright ion [in the ideal case $B(n_i)$ is a Poisson distribution with mean count per sub-bin $R_B t_s$]. The calculation of $p_D = P(\{n_i\}|\text{dark})$ is more involved, because we must sum over the possibilities that the ion decayed after or during the detection time $t_b = Nt_s$. To a good approximation

$$p_D = \left(1 - \frac{t_b}{\tau}\right)\prod_{i=1}^{N} D(n_i) + \left(\frac{t_s}{\tau}\right)\sum_{j=1}^{N}\prod_{i=1}^{j-1} D(n_i)\prod_{i=j}^{N} B(n_i)$$

where $(1 - t_b/\tau)$ is the probability the ion decays after the last sub-bin, (t_s/τ) the probability it decays during any particular sub-bin j, and $D(n_i)$ the background count distribution with mean $R_D t_s$. Using a recursion relation

$$p_D = (1 - t_b/\tau)M_N + (t_s/\tau)S_N;$$
$$M_0 = 1, \qquad M_k = M_{k-1}D(n_k); \qquad (1)$$
$$S_0 = 0, \qquad S_k = (S_{k-1} + M_{k-1})B(n_k)$$

reduces the calculation of p_D from $O(N^2)$ to $O(N)$ operations, making real-time readout much faster. We have made the simplifying approximations that $t_s, t_b \ll \tau$, and that the mean count rate changes from R_D to R_B at the start of the sub-bin j in which the ion decays; similar expressions are found if these approximations are not made, with negligible effect on the results.
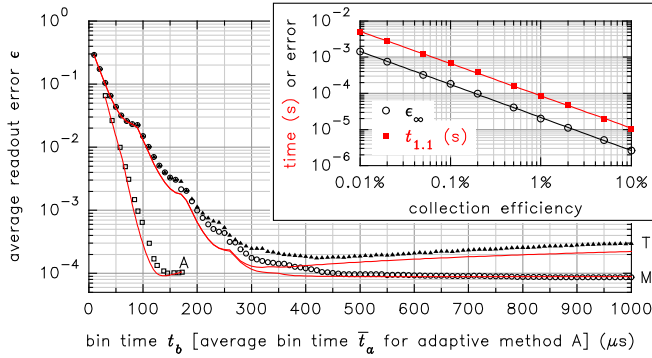
FIG. 2 (color online).   Average readout error ϵ versus readout time for the $^{40}\text{Ca}^+$ optical qubit, for three different analysis methods. Analyses of the experimental data are plotted as symbols; statistical uncertainty is at most the size of the symbols. The accompanying curves are simulations of 10^9 trials using ideal Poisson statistics. Cusps arise from the discrete nature of photon counting. T: photon-count threshold method, where the threshold n_c was optimized for each bin time. M: maximum likelihood method. A: adaptive maximum likelihood method. Inset: Simulations using method M, showing the asymptotic average error ϵ_∞ and the time $t_{1.1}$ required to reach $\epsilon = 1.1\epsilon_\infty$ as functions of the net photon collection efficiency.

The results of applying the maximum likelihood method to the same data set are also shown in Fig. 2. For $B(n_i)$ and $D(n_i)$, Poisson distributions were convolved with the PMT dark count distribution [17]. We see that for $t_b \gtrsim 200\ \mu\text{s}$ the maximum likelihood method gives a lower error than the threshold method, tending to an asymptotic value $\epsilon = 0.87(11) \times 10^{-4}$ [with $\epsilon_D = 1.5(2) \times 10^{-4}$], or a fidelity 99.9913(11)%. Furthermore, the maximum likelihood method does not require a precise choice of parameters (n_c, t_b) which must be determined from control data; we only need to know the independently measured rates R_B and R_D, and to choose a sufficiently long t_b. The observed error is compared with that from a simulation of 10^9 trials using ideal Poisson statistics in Fig. 2: although at short t_b the experimental ϵ is greater due to super-Poissonian noise in the data, at long t_b it converges to the simulation's asymptote at $\epsilon = 0.89 \times 10^{-4}$. We conclude that, at optimum t_b, the maximum likelihood method is less sensitive to experimental noise (e.g., cosmic ray events, drift in R_B) than the threshold method.

We now discuss faster detection by using an adaptive version of the maximum likelihood technique [11]. In the preceding discussion, the detection bin length $t_b = Nt_s$ was fixed and we evaluated the likelihoods p_B, p_D at the end of the bin, deciding that the ion was dark if $p_D > p_B$. However, the absolute values of p_B and p_D also contain useful information. The *estimated* error probability e_D that we have incorrectly deduced the ion to be dark when $p_D > p_B$ is given by Bayes' theorem [18]:

$$e_D = 1 - P(\text{dark}|\{n_i\}) = 1 - \frac{P(\{n_i\}|\text{dark})}{P(\{n_i\})} = \frac{p_B}{p_B + p_D}$$

and similarly for e_B in the case where $p_B \gtrsim p_D$. By evaluating p_D and p_B at the end of each sub-bin, we can terminate the detection bin at $t_a < t_b$ when the estimated error probability e_B or e_D falls below some chosen cutoff threshold e_c. We also impose a cutoff time $t_c \leq t_b$ in case the error threshold is not reached; t_c is thus the worst case readout time. The result is that, for a given desired error level, the average detection bin length $\bar{t}_a$ is shorter than when the bin length is fixed. If e_c is not reached, e_B or e_D still quantifies confidence in the measurement outcome, useful for QEC. Using the recursion relations (1) we can evaluate p_B, p_D in $<1\ \mu\text{s}$, while each sub-bin is in progress, so there is negligible time overhead.

For our conditions we find that, at little cost to ϵ, faster detection can be obtained by omitting the effect of spontaneous decay in the analysis, i.e., using $p_D = \Pi_{i=1}^N D(n_i)$. An adaptive analysis of the same data set is shown in Fig. 2, for $t_c = 500\ \mu\text{s}$ and a range of threshold values $10^{-6} \leq e_c \leq 10^{-1}$. For each e_c we plot the experimentally measured average error ϵ against $\bar{t}_a$. For an average readout time of $\bar{t}_a = 145\ \mu\text{s}$, the error reaches $\epsilon = 1.0(1) \times 10^{-4}$, which is about 35 times lower than the nonadaptive maximum likelihood method, or over 3 times as fast for the same ϵ. The average readout time for the bright (dark) state is 72 μs (219 μs).

For all of the analysis methods described, the bright $S_{1/2}$ state can be detected more accurately than the dark $D_{5/2}$ state because the known bright $\rightarrow$ dark transfer rate is so low (we measure it to be $<10^{-3}\ \text{s}^{-1}$). The data imply the bright state can be detected with over 99.9998% fidelity, $\epsilon_B < 2 \times 10^{-6}$, in average time $\bar{t}_a = 91\ \mu\text{s}$ [while retaining $\epsilon_D = 2.5(2) \times 10^{-4}$ in $\bar{t}_a = 292\ \mu\text{s}$]. This asymmetric readout error could be exploited for QEC.

The optical qubit offers high-fidelity readout but it suffers from two drawbacks: a finite lifetime τ and the need for high frequency stability in the optical domain. Qubits stored in hyperfine ground states avoid these problems and exhibit some of the longest coherence times ever measured [5,8]. We turn now to the implementation of state detection for a qubit stored in the $|\uparrow\rangle = S_{1/2}^{3,+3}$ and $|\downarrow\rangle = S_{1/2}^{4,+4}$ hyperfine ground states of $^{43}\text{Ca}^+$ (where the superscripts give the quantum numbers F, M_F). For readout, we first map this hyperfine qubit to the optical qubit by state-selective transfer $|\downarrow\rangle \rightarrow D_{5/2}$.

We Doppler cool a single $^{43}\text{Ca}^+$ ion on the $S_{1/2}^3 \leftrightarrow P_{1/2}^4$ and $S_{1/2}^4 \leftrightarrow P_{1/2}^4$ transitions. State preparation of $|\downarrow\rangle$ is by optical pumping with σ^+ polarized light on the same transitions. Preparation of $S_{1/2}^{3,M_F}$ is achieved by extinguishing the $S_{1/2}^3 \leftrightarrow P_{1/2}^4$ beam before the $S_{1/2}^4 \leftrightarrow P_{1/2}^4$ beam: this prepares a statistical mixture of M_F states rather than $|\uparrow\rangle$ but the calculated effect on the measured readout error is $<10^{-4}$. To map $|\downarrow\rangle$ to the $D_{5/2}$ shelf the ion is illuminated with 393 nm σ^+ light which drives $|\downarrow\rangle \leftrightarrow P_{3/2}^{5,+5}$. This results in optical pumping to $D_{5/2}$ or $D_{3/2}$ with branching ratios 5.3% and 0.63%, respectively [13]. Light
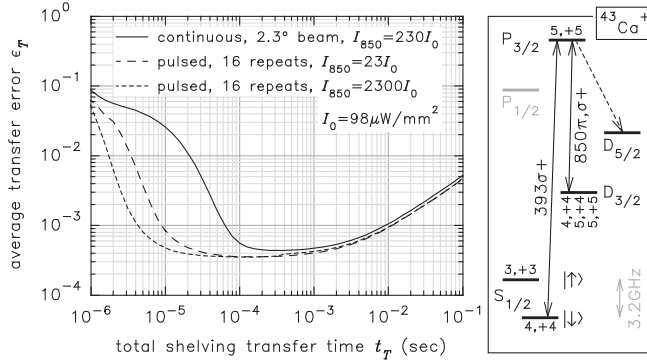
FIG. 3. Rate equation simulations for the ^{43}Ca$^+$ shelving transfer $(|\uparrow\rangle, |\downarrow\rangle) \rightarrow (|\uparrow\rangle, D_{5/2})$. The optimum average shelving transfer error ϵ_T is shown versus total time t_T allowed for the transfer, for both continuous and pulsed methods. The 393 nm intensity and (in the pulsed method) all pulse durations were numerically optimized for each t_T. The error increases at short t_T due to higher 393 nm intensity causing off-resonant shelving of $|\uparrow\rangle$; at long t_T the error increases because of decay from the $D_{5/2}$ shelf. The minimum error is 3.5×10^{-4} at $t_T = 160$ μs; for $t_T = 10$ μs an error of 4.8×10^{-4} is available. Right: Simplified ^{43}Ca$^+$ level diagram; states relevant to the shelving transfer are labeled by F, M_F.

at 850 nm containing σ^+ and π polarizations is used to empty the relevant $D_{3/2}$ states via the $P_{3/2}^{5,+5}$ state (Fig. 3, right). Assuming perfect repumping from $D_{3/2}$, the situation reduces to that for ions without low-lying D levels, but with the important difference that we only need to drive enough transitions to transfer $|\downarrow\rangle$ to the shelf (rather than to collect fluorescence) before off-resonant excitation of $|\uparrow\rangle$ occurs; since the $P_{3/2} \rightarrow D_{5/2}$ branching ratio is much greater than typical photon collection efficiencies this gives a significant advantage.

To optimize parameters the shelving transfer process was modeled by rate equations applied to the entire 144-state ($4S$, $4P$, $3D$) manifold. The optimum shelving method would be a repeated sequence of three laser pulses (393 nm σ^+, 850 nm σ^+, 850 nm π), since then there is negligible probability of the ion decaying to $|\uparrow\rangle$. The main limitation is off-resonant (by 3.1 GHz) excitation of $|\uparrow\rangle \leftrightarrow P_{3/2}^{4,+4}$. Continuous excitation allows similar fidelity if the 850 nm π component is weak (though with slower shelving; see Fig. 3). Accordingly, in the experiment, we used a single circularly polarized 850 nm beam travelling at a small angle (2.3°) to the quantization axis, giving polarization components with intensities $(I_{\sigma^+}, I_\pi, I_{\sigma^-}) = (0.9992, 0.0008, 2 \times 10^{-7}) \times 230(70)I_0$, where the saturation intensity $I_0 = 98$ μW/mm^2. The shelving transfer was accomplished with a single simultaneous 393 nm + 850 nm pulse, with duration set to the optimum value predicted by the model, $t_T = 400$ μs. No improvement was found by varying t_T or by using alternating 393 and 850 nm pulses (to avoid two-photon effects, which are not modeled by the rate equations). After shelving, state de-

tection proceeds as for ^{40}Ca$^+$; photon-count thresholding with $t_b = 2$ ms was used as the optical qubit readout is not the limiting factor.

The net average readout error for the hyperfine qubit was measured from 20 000 trials to be $\epsilon_{hfs} = \frac{1}{2}(\epsilon_\uparrow + \epsilon_\downarrow) = 2.3(3) \times 10^{-3}$, a fidelity of 99.77(3)%. [The error for the $|\uparrow\rangle$ state was $\epsilon_\uparrow = 1.7(4) \times 10^{-3}$.] A separate experiment measured the optical qubit readout error to be $1.0(2) \times 10^{-3}$, significantly poorer than for ^{40}Ca$^+$ due to a lower fluorescence rate $R_B = 7500$ s^{-1} (caused partly by coherent population trapping effects, which could be eliminated by polarization modulation techniques [19]). This implies an average error $\epsilon_T = 1.3(4) \times 10^{-3}$ for the shelving transfer. This is somewhat above the modeled value of 0.44×10^{-3}; possible reasons for this include imperfect circular polarization of the 850 nm beam, imperfect population preparation, and broadening of the 393 nm transition (e.g., due to finite laser linewidth).

In conclusion, we demonstrate fast, direct, single-shot readout from optical and hyperfine trapped-ion qubits at fidelities comparable with those required for a fault-tolerant QC. An adaptive detection method reduced the optical qubit readout error by a factor ≈ 35 for a given average detection time, reaching 99.99% fidelity in 145 μs, with negligible time overhead due to the classical control system. A simple, robust method for readout of hyperfine qubits, capable of comparable fidelity and speed, was proposed and implemented. An increase in the photon collection efficiency by an order of magnitude, to 2%, would speed up both readout methods, and reduce the optical qubit readout error, by a similar factor (Fig. 2, inset).

[1] E. Knill, Nature (London) **434**, 39 (2005).
[2] A. M. Steane, Quantum Inf. Comput. **7**, 171 (2007).
[3] M. A. Nielsen, Rep. Math. Phys. **57**, 147 (2006).
[4] C. Monroe et al., in Atomic Physics 17, edited by P. De Natale (AIP Press, New York, 2001), p. 173.
[5] C. Langer et al., Phys. Rev. Lett. **95**, 060502 (2005).
[6] M. Acton et al., Quantum Inf. Comput. **6**, 465 (2006).
[7] S. Olmschenk et al., Phys. Rev. A **76**, 052314 (2007).
[8] D. M. Lucas et al., arXiv:quant-ph/0710.4421v1.
[9] C. Wunderlich et al., J. Mod. Opt. **54**, 1541 (2007).
[10] D. J. Wineland et al., Opt. Lett. **5**, 245 (1980).
[11] D. B. Hume et al., Phys. Rev. Lett. **99**, 120502 (2007).
[12] The readout method is not sensitive to the choice of M_J.
[13] P. Barton et al., Phys. Rev. A **62**, 032503 (2000).
[14] J. Gambetta et al., Phys. Rev. A **76**, 012325 (2007).
[15] M. C. Teich et al., Phys. Rev. D **36**, 2649 (1987).
[16] C. Langer, Ph.D. thesis, University of Colorado, 2006.
[17] We neglect time correlations caused by the cosmic rays.
[18] T. Bayes, Phil. Trans. R. Soc. London **53**, 370 (1763).
[19] M. G. Boshier et al., Appl. Phys. B **71**, 51 (2000).